AIChE WILEY InterScience DISCOVER SOMETHING GREAT

STR-PEM Fuel Cell as a Reactor Building Block

Ee-Sunn J. Chia, Jay B. Benziger, and Ioannis G. Kevrekidis
Dept. of Chemical Engineering, Princeton University, Princeton, NJ 08544

DOI 10.1002/aic.10987
Published online September 26, 2006 in Wiley InterScience (www.interscience.wiley.com).

The dynamics of the stirred tank reactor polymer electrolyte membrane (STR-PEM) fuel cell arise from the balance between water production and water removal within the cell. This results in STR-PEM fuel cell steady-state multiplicity, remarkably analogous to that of an autocatalytic exothermic STR. Model flooding effects in the cathodeside catalyst/gas diffusion layer by accounting for relevant mass-transport processes is presented. We use the resulting STR-PEM fuel cell model as a building block to construct approximations of more conventional integral (plug flow) type fuel-cell reactors. This approach bypasses more complicated, distributed gas diffusion layer models. Connecting several STR-PEM fuel cells in series, the effects of four operating parameters (temperature, external load resistance, inlet hydrogen and inlet oxygen flow rates) on the current evolution in each tank can be monitored and rationalized. © 2006 American Institute of Chemical Engineers
AIChE J, 52: 3902–3910, 2006
Keywords: PEM fuel cell, steady-state multiplicity, stirred-tank reactor

Introduction

Recent developments in polymer electrolyte membrane (PEM) fuel cell technology lend support to the prospect of utilizing PEM fuel cells for mobile and stationary applications.[1–3] Before PEM fuel cells become a commercially viable alternative power source, however, it is critical that predictive models of fuel cell dynamic performance under realistic operating conditions become further developed. Many PEM models attempt to capture the internal workings of an operating fuel cell.[4–8] However, such models often include intricate phenomenological details that create additional complexity. We have previously designed, constructed, and experimentally operated a *differential* PEM fuel cell.[9–11] This simplified version of an operating PEM fuel cell retains the essential physics that enable us to study the kinetics and dynamics of the fuel cell.[12,13]

We have previously described the remarkable analogy between the energy balance in the classical exothermic stirred-tank reactor,[14–18] and the water balance in the *differential* PEM fuel cell.[9] Water production within the fuel cell improves proton transport through the PEM, and thereby, autocatalytically accelerates the reaction. The balance between water production and water removal in the stirred tank reactor-fuel cell (STR-PEM) gives rise to multiple steady-states as indicated by the intersections of the water removal and water production curves (corresponding to heat production and heat removal curves in the CSTR heat balance).

This article is organized as follows. First, we extend our initial STR-PEM fuel cell model to incorporate key mass-transport processes that successfully capture flooding effects in the cathode side catalyst/gas diffusion layer. We then employ our one-dimensional (1-D) stirred-tank reactor model via a "tanks in series" approach as a building block to build approximations of more complex flow geometries. By using well established computational tools, such as dynamic simulation, continuation, and bifurcation analysis,[19–22] we study the STR-PEM fuel cell dynamics and its parametric operation. This provides a simplified, straightforward approach to examine dynamics of PEM fuel cells. We have bypassed the more complex, spatially distributed gas diffusion layer models with an eye towards easier handling of the dynamics.[23–25] We conclude with a summary and brief discussion of the results.

STR-PEM fuel cell

The hydrogen-oxygen STR-PEM fuel cell consists of the anode, and the cathode flow channels, sandwiching the mem-

Correspondence concerning this article should be addressed to J. B. Benziger at benziger@princeton.edu.
I. G. Kevrekidis is also affiliated with Program in Applied and Computational Mathematics, Princeton University, Princeton, NJ 08544.

© 2006 American Institute of Chemical Engineers

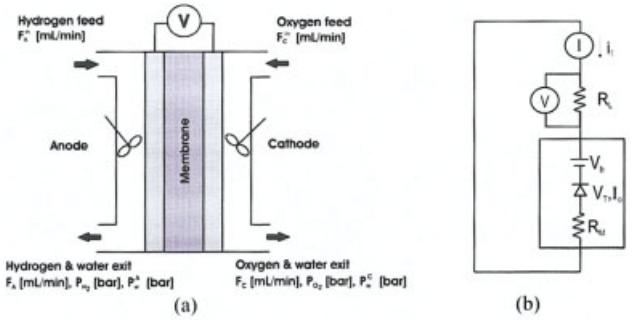

Figure 1. STR-PEM fuel cell model.

(a) Nonhumidified hydrogen and oxygen are fed to the anode and cathode chambers that act as stirred tank reactors. Unreacted gases and product water exit from both sides, and (b) the equivalent electrical circuit for the STR-PEM fuel cell. The membrane resistance (R_M) depends on the membrane water content while the external load resistance (R_L) is a controllable parameter. [Color figure can be viewed in the online issue, which is available at www.interscience.wiley.com.]

brane electrode assembly. As shown in Figure 1a, the flow channels are modeled as stirred-tank reactors, to which hydrogen and oxygen are fed at fixed flow rates of F_A^{in} and F_C^{in} (m^3/s). The STR-PEM fuel cell is electrically connected to an external load resistance R_L (Ω). Aside from controlling the inlet flow rates and load resistance, we assume that the fuel cell temperature, T (K) can be controlled.* Figure 1b illustrates that the current through, and the voltage drop across the external load are measurable quantities. The membrane resistance R_M (Ω), which is a strong function of the membrane water content, but only weakly dependent on temperature, represents the resistance to proton transport.[26–31] Previous models of PEM fuel cells have employed a linearized relationship between membrane resistance and water content.[32] Those linearized models cannot capture steady-state multiplicity and current ignition in PEM fuel cells, and so it is necessary to use models that can capture that physics. V_b (Volt) is the potential due to the *chemical potential* gradient of hydrogen between the two electrodes.

We have focused on modeling four regions within the STR-PEM fuel cell as illustrated in Figure 2. This diagram highlights the important mass-transport processes occurring within the anode flow channel, membrane, cathode side catalyst/gas diffusion layer, and the cathode flow channel. The system variables include the hydrogen and water partial pressures in the anode flow channel, P_{H_2} and P_w^A (Pa), the membrane water activity a_w, the moles of water in the gas diffusion layer $n_{w,gdl}$,[33] and the partial pressures of oxygen and water in the cathode flow channel, P_{O_2} and P_w^C (Pa).

We have built a model PEM fuel cell with a segmented anode to test our model; results from the experiments are reported elsewhere.[13,34] The parameters in the computations presented here are based on the laboratory segmented anode PEM fuel cell, as well as on experimental results with our STR fuel cell reactor. The anode catalyst/gas diffusion layer mass-transport effects are lumped into the effective mass transfer coefficient k (estimated at 1.3×10^{-2} mol/m^2-s) that governs the rate of water transport between the membrane, and the anode flow channel. This rate of water transport is determined by the gradient in water activity and expressed by $kA(a_w - a_w^A)$, where A is the membrane area of 1.5×10^{-4} m^2, a_w is the membrane water activity, and a_w^A is the anode flow channel water activity. The anode flow channel water activity is expressed as the ratio of the water partial pressure in the anode flow channel P_w^A, to the water vapor pressure at the fuel cell temperature P_{wo} as $a_w^A = P_w^A/P_{wo}$. The model also includes an electro-osmotic drag of water from the anode flow channel through the term $k_w^{eo}(i/\mathcal{F})$. The electro-osmotic mass-transfer coefficient has been experimentally found to depend stronger than linearly on the water activity in the membrane[32,35–37]; the data were approximated by the form $k_w^{eo} = 2(a_w^A)^4 = 2(P_w^A/P_{wo})^4$. Most of our results found electro-osmotic drag was only important at large current densities (>1 A/cm^2),[38] and were not important for most of the conditions studied in this article.

We will refer to the cathode catalyst/gas diffusion layer as the cathode GDL. Water produced at the cathode catalyst (effectively part of the GDL), can either enter the membrane or the cathode-flow channel. The rate of water transport between the cathode GDL, and the membrane depends on the gradient in water activity between the GDL, and the membrane as described by $k'A(a_{gdl} - a_w)$ where a_{gdl} is the GDL water activity, and k' (estimated at 5.6×10^{-2} mol/m^2-s) is the effective mass transfer coefficient for water transport between the GDL, and the membrane. Similarly, water from the GDL is transported to the cathode flow channel at a rate of $k''A(a_{gdl} - a_w^C)$, where k'' (estimated at 1.6×10^{-2} mol/m^2-s) is the corresponding mass-transfer coefficient; this rate depends on the difference between GDL water activity, and cathode flow channel water activity a_w^C. The latter can be expressed in terms

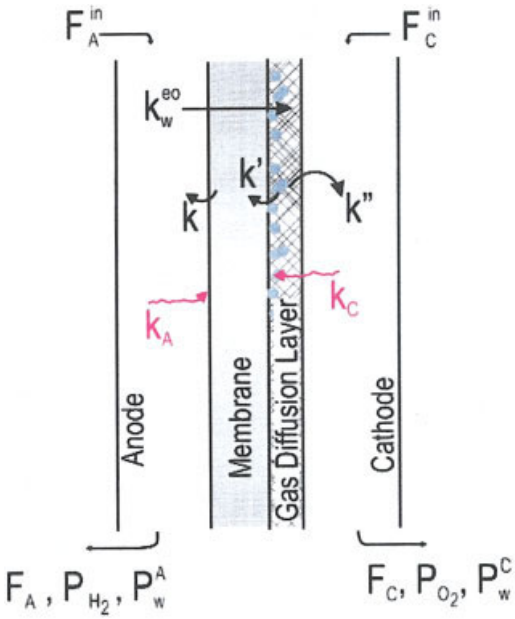

Figure 2. Water transport processes.

The model consists of four regions with water being produced in the cathode catalyst layer (effectively part of the cathode GDL). The anode GDL is ignored here since in these studies the fuel cell operates under dry anode conditions. [Color figure can be viewed in the online issue, which is available at www.interscience.wiley.com.]

*For the single fuel cell models, temperature gradients are assumed small. The assumption of constant temperature must be relaxed for fuel cell stacks.

of the water partial pressure in the cathode flow channel as $a_w^C = P_w^C/P_{wo}$.

Flooding effects at the cathode

The mass-transfer coefficients that govern the rate of H_2 transport to the anode catalyst, and O_2 transport to the cathode catalyst are, respectively k_A (estimated at 5.8×10^{-6} mol/m^2-s-Pa) and k_C, for which values are estimated later. At steady state, the rate of mass transfer to the catalyst must equal the rate of reaction occurring at the catalyst surface; the reactant partial pressures at the electrode/electrolyte interface $P_{H_2}^{cat}$ and $P_{O_2}^{cat}$ (Pa) are reduced from those in the flow channels due to mass transfer across the GDL and can be expressed as

$$P_{H_2}^{cat} = P_{H_2} - \frac{i}{2\mathcal{F}k_A A}; \; P_{O_2}^{cat} = P_{O_2} - \frac{i}{4\mathcal{F}k_C A} \tag{1}$$

where $\mathcal{F}$ represents Faraday's constant. Water is produced on the cathode side; we limit our model to conditions where there is no liquid water in the flow channels at the anode-side, so that k_A remains constant. At the cathode, our model allows for liquid water to accumulate *within the catalyst layer,* creating an additional mass-transport resistance for O_2. In what follows, and for our experimental system, the maximum moles of gaseous water that can exist in the catalyst/GDL layer is found as $n_w^{G,\max} = P_{wo}V_{gdl}/RT$ where V_{gdl} is our GDL void volume of 7.5×10^{-8} m^3 estimated from an area of 1.5×10^{-4} m^2, a thickness of 10^{-3} m, and a porosity of 0.5. Without liquid water, the mass transfer of oxygen to the catalyst occurs at the maximum possible value of $k_C^{\max}$ (estimated at 5.8×10^{-7} mol/m^2-s-Pa from a gas phase diffusion coefficient of 10^{-5} m^2/s, a layer thickness of 10^{-3} cm, a tortuosity factor of 3, and a void fraction of 0.5). However, k_C decreases significantly at the onset of liquid water formation at the cathode GDL and approaches a minimum rate of $k_C^{\min}$ (5.8×10^{-10} mol/m^2-s-Pa) when the GDL is completely filled with liquid water at $n_w^{\max}$ (8.3×10^{-4} moles for our V_{gdl}).* We express k_C (as depicted schematically in Figure 3) as a function of the moles of liquid water present in the GDL n_w^L [33]

$$k_C = \frac{k_c^{\max}}{1 + \dfrac{n_w^L}{n_w^{\max}}\left(\dfrac{k_c^{\max} - k_c^{\min}}{k_c^{\min}}\right)} \tag{2}$$

The battery voltage V_b depends on the thermodynamic potential at standard conditions V_o (1.23 V), the compositions in both the anode and cathode, and the total pressure in each flow channel P_T (10^5 Pa). The electron transfer reactions at the anode and cathode are equivalent to chemical diodes, described through typical Butler-Volmer kinetics. From the equivalent electrical circuit in Figure 1b, the diode effect is captured in the second term in the following equation (where $V_T = 0.05$ V is the diode threshold voltage while $I_o = 0.002$ A is the diode saturation current). The effective fuel cell voltage V_{FC} (Volt) is derived from the equivalent circuit in Figure 1b as

$$V_{FC} = V_b - V_T \ln\left(1 + \frac{i}{I_O}\right) \quad \text{where} \quad V_b = V_o + \frac{RT}{4\mathcal{F}} \ln \frac{(P_{H_2,anode}^{cat}/P_T)^2 (P_{O_2,cathode}^{cat}/P_T)}{(a_{gdl})^2} \tag{3}$$

The explicit Butler-Volmer kinetics only need to be considered at very small currents. Above current densities of ~0.05 A/cm^2 the diode may be approximated as a constant threshold voltage, so the fuel cell voltage is approximately the battery voltage reduced by $\sim 3V_T$.

Mass balances

It has been shown previously that the membrane resistance depends strongly on the membrane water activity.[30] For a membrane with thickness l (1.27×10^{-4} m), and area A (1.5×10^{-4} m^2) the membrane resistance can be correlated as

$$R_M(a_w) = 10^5 \exp(-14 a_w^{0.2}) \frac{l}{A} \quad (\Omega) \tag{4}$$

The fuel cell current is expressed as

$$i = \frac{V_{FC}}{R_M(a_w) + R_L} \quad (\text{A}) \tag{5}$$

Writing the mass balances for relevant species in each respective region, we obtain the following set of equations (6 thru 9). Equations 6 and 7 describe the balance of hydrogen in the anode and oxygen in the cathode while Eqs. 8 and 9 describe the inventory of water in the membrane and GDL, respectively.

When there is only water vapor present in the GDL, the water activity is the ratio of the partial pressure of water in the GDL to the water vapor pressure $a_{gdl} = P_w^{gdl}/P_{wo}$. The partial pressure of water in the GDL, can be related to the moles of gaseous water in the GDL ($n_{w,gdl}$) so that the activity can be expressed as $a_{gdl} = (n_{w,gdl}RT)/(V_{gdl}P_{wo})$. When the GDL water activity becomes equal to 1, liquid water starts accumulating in the GDL (see Figure 3). In the following equations N_{SO_3} is the moles of sulfonic acid groups in the membrane (3.5×10^{-5} mol), λ is the membrane water content expressed as the number of water molecules per sulfonic acid group,[30] while V_g^A and V_g^C are the anode, and cathode flow channel volumes (2×10^{-7} m^3)

$$\frac{V_g^A}{RT}\frac{dP_{H_2}}{dt} = F_A^{in}\frac{P_{H_2}^{in}}{RT} - F_A\frac{P_{H_2}}{RT} - \frac{i}{2\mathcal{F}} \tag{6}$$

$$\frac{V_g^C}{RT}\frac{dP_{O_2}}{dt} = F_C^{in}\frac{P_{O_2}^{in}}{RT} - F_C\frac{P_{O_2}}{RT} - \frac{i}{4\mathcal{F}} \tag{7}$$

$$N_{SO_3}\frac{d\lambda}{da_w}\frac{da_w}{dt} = k'A(a_{gdl} - a_w) - kA\left(a_w - \frac{P_w^A}{P_{wo}}\right) \tag{8}$$

*In this idealization, water floods the GDL. Actually, water will only flood the thin catalyst layer between the *hydrophobic* GDL, and the membrane.

$$\frac{dn_{w,gdl}}{dt} = \frac{i}{2\mathcal{F}} - k'A(a_{gdl} - a_w) - k''A\left(a_{gdl} - \frac{P_w^C}{P_{wo}}\right) + k_w^{eo}\frac{i}{\mathcal{F}} \quad (9)$$

$$\lambda = 14.9a_w - 44.7a_w^2 + 70.0a_x^3 - 29.5a_w^4 - 0.446a_w^5 \quad (10)$$

Our estimates of the mass-transfer coefficients are obtained from fitting experimental data from the autohumidified STR-PEM fuel cell.[9,12,38] Experimental values for water production and water removal were determined. Water production being 1/2 the current and water removal is the product of the water partial pressure (determined from the relative humidity of the effluents), and the gas-flow rates at the anode and cathode. Water is formed at the cathode/membrane interface; we assume a negligible water activity gradient across the gas diffusion layer so the water activity in the cathode gas diffusion layer (GDL) is the same as at the cathode/membrane interface. The flux of water exiting the cathode side by convection must equal the water flux from the cathode GDL to the cathode flow channel $k''(a_w^{GDL} - a_w^C)$. The convective flux of water leaving the anode is equal to the flux from the cathode GDL to the anode-flow channel. Assuming resistances in series from the cathode GDL to the membrane (k'), and from the membrane to the anode flow channel (k) the overall flux from the cathode GDL to the anode flow channel is $[kk'/(k + k')](a_w^{GDL} - a_w^A)$. As an initial estimate, we assumed that *liquid* water is present at the cathode GDL, so that a_w^{GDL} is 1. Based on the convective water fluxes in the anode, and cathode effluents se determined that k'', and the lumped mass-transfer coefficient $kk'/(k + k')$, were both on order of 10^{-2} mol/m^2-s. We chose values of k, k' and k'' given in the notation section to be consistent with the data, but no optimization was done in determining these values.

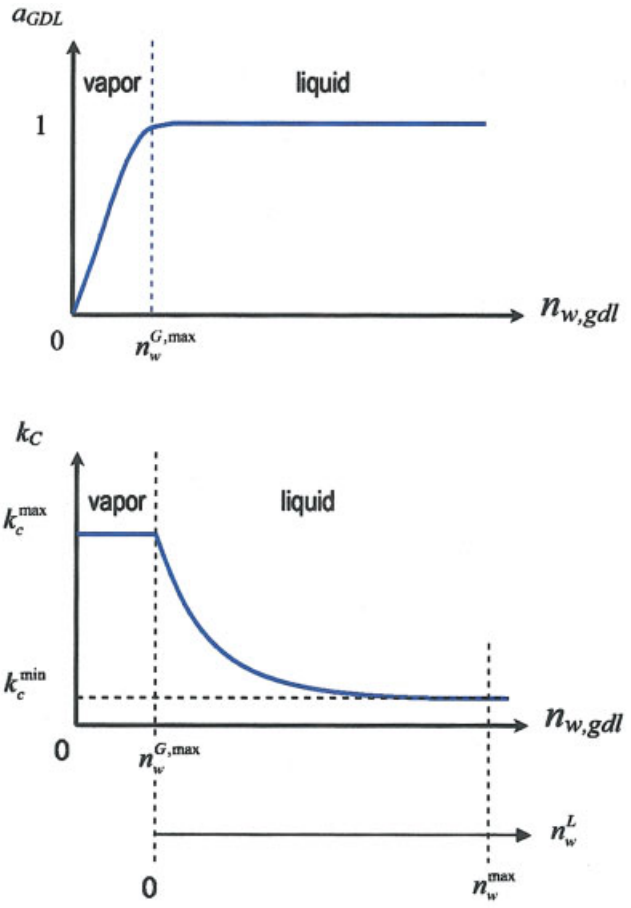

Figure 3. Cathode GDL mass transfer.

Oxygen mass transport to the cathode electrode decreases rapidly after the onset of liquid water formation. When liquid water appears within the layer (so that a_{gdl} is 1), k_C will start decreasing and eventually will approach $k_C^{\min}$. [Color figure can be viewed in the online issue, which is available at www.interscience.wiley.com.]

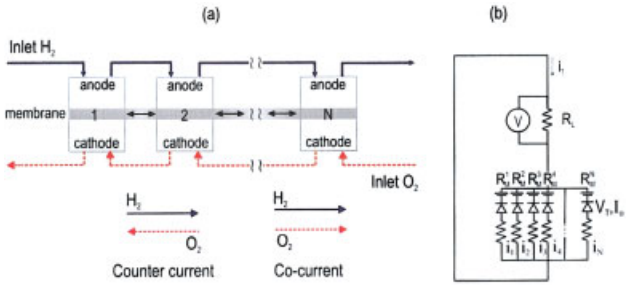

Figure 4. Building blocks.

(a) Several STR-PEM fuel cells can be connected in series to approximate more complicated, spatially distributed flow schemes, and (b) STR-PEM fuel cell electrical circuit equivalent, with the fuel cell membrane resistances electrically connected in parallel to one another. [Color figure can be viewed in the online issue, which is available at www.interscience.wiley.com.]

We will consider the case of constant pressure operation in each flow channel ($P_T = 10^5$ Pa), with pure reactant inlet flow rates specified by F_A^{in} and F_C^{in}. Therefore, the partial pressures of water in the anode and cathode can be expressed, as $P_w^A = P_T - P_{H_2}$ and $P_w^C = P_T - P_{O_2}$. The exit flow rates on both the anode and cathode sides are F_A and F_C (m^3/s). In the anode, the respective terms in the expression for F_A represent the moles of hydrogen entering the fuel cell, the rate of water transferred between the membrane and the anode flow channel, the rate of water electro-osmotically dragged away from the anode, and the rate of water production. Similarly, F_C in the cathode depends on the moles of oxygen entering the cathode flow channel, the rate of water transferred between the cathode GDL, and the cathode flow channel, in addition to the rate of oxygen consumption

$$F_A = \left[F_A^{in}\frac{P_T}{RT_{in}} + kA\left(a_w - \frac{P_w^A}{P_{w0}}\right) - \frac{i}{\mathcal{F}}(k_w^{eo} + 0.5)\right]\frac{RT}{P_T} \quad (11)$$

$$F_C = \left[F_C^{in}\frac{P_T}{RT_{in}} + k''A\left(a_{gdl} - \frac{P_w^C}{P_{wo}}\right) - 0.25\frac{i}{\mathcal{F}}\right]\frac{RT}{P_T} \quad (12)$$

Tanks in Series

Figure 4a depicts how the STR-PEM fuel cell (a "differential element"), when connected in series, can be used to model other more complicated flow fields. We will illustrate the flow effects by feeding the reactants from opposite ends (countercurrent), and from the same end (cocurrent) of the fuel cell reactor. The fuel cells are physically connected in series, but electrically the fuel cell membrane resistances are *parallel* to

each other (see Figure 4b). In the cocurrent-flow scheme, the anode and cathode exit streams from tank $j-1$, are also the inlet streams into tank j. Therefore, the exiting flow rates in the anode and cathode for each tank depend on the flow rates of the previous tank. In addition, water can be transported through the membrane from tank to tank; the corresponding coupling term is modeled by $k_m A_m(a_{w(j-1)} - a_{w(j)})$, where k_m (0.5 mol/m^2-s) is the mass-transfer coefficient for water through the membrane between different tanks, and A_m (1×10^{-6} m^2) is the membrane area available for longitudinal water transport.

Similar to the single STR-PEM fuel cell, we operate under constant total pressure, so that the partial pressures of water in the anode and cathode for each tank is $P^A_{w(j)} = P_T - P_{H_2(j)}$, and $P^C_{w(j)} = P_T - P_{O_2(j)}$. For several STR-PEM fuel cells connected in cocurrent flow, the equations are written as follows for tanks $j = 1 \cdots N$. For multiple tanks in series $A_{(j)} = A/N$

$$\frac{(V^A_g/N)}{RT}\frac{dP_{H2(j)}}{dt} = F_{A(j-1)}\frac{P_{H2(j-1)}}{RT} - F_{A(j)}\frac{P_{H2(j)}}{RT} - \frac{i_{(j)}}{2\mathcal{F}} \quad (13)$$

$$\frac{(V^C_g/N)}{RT}\frac{dP_{O_2(j)}}{dt} = F_{C(j-1)}\frac{P_{O_2(j-1)}}{RT} - F_{C(j)}\frac{P_{O_2(j)}}{RT} - \frac{i_{(j)}}{4\mathcal{F}} \quad (14)$$

$$\frac{N_{SO_3}}{N}\frac{d\lambda}{da_{w(j)}}\frac{da_{w(j)}}{dt} = k'A_{(j)}(a_{gdl(j)} - a_{w(j)}) - kA_{(j)}\left(a_{w(j)} - \frac{P_{wA(j)}}{P_{w0}}\right) + k_m A_m(a_{w(j-1)} - a_{w(j)}) - k_m A_m(a_{w(j)} - a_{w(j+1)}) \quad (15)$$

$$\frac{dn_{gdl(j)}}{dt} = \frac{i_{(j)}}{2\mathcal{F}} - k'A_{(j)}(a_{gdl(j)} - a_{w(j)}) - k''A_{(j)}\left(a_{gdl(j)} - \frac{P_{wC(j)}}{P_{w0}}\right) + k^{eo}_{w(j)}\frac{i_{(j)}}{\mathcal{F}} \quad (16)$$

$$F_{A(j)} = \left[F_{A(j-1)}\frac{P_T}{RT} + kA_{(j)}\left(a_{w(j)} - \frac{P^A_{w(j)}}{P_{w0}}\right) - \frac{i_{(j)}}{\mathcal{F}}(k^{eo}_{w(j)} + 0.5)\right]\frac{RT}{P_T} \quad (17)$$

$$F_{C(j)} = \left[F_{C(j-1)}\frac{P_T}{RT} + k''A_{(j)}\left(a_{gdl(j)} - \frac{P^C_{w(j)}}{P_{w0}}\right) - 0.25\frac{i_{(j)}}{\mathcal{F}}\right]\frac{RT}{P_T} \quad (18)$$

$$V_{FC(j)} = V_o + \frac{RT}{4\mathcal{F}}\ln\frac{(P^{cat}_{H2(j)}/P_T)^2(P^{cat}_{O2(j)}/P_T)}{(a_{gdl(j)})^2} - V_T\ln\left(1 + \frac{i_{(j)}}{I_o}\right) \quad (19)$$

$$i_{(j)} = \frac{V_{FC(j)} - V}{R_{M(j)}} \quad (20)$$

$$V = R_L\sum_{j=1}^{N} i_{(j)} \quad (21)$$

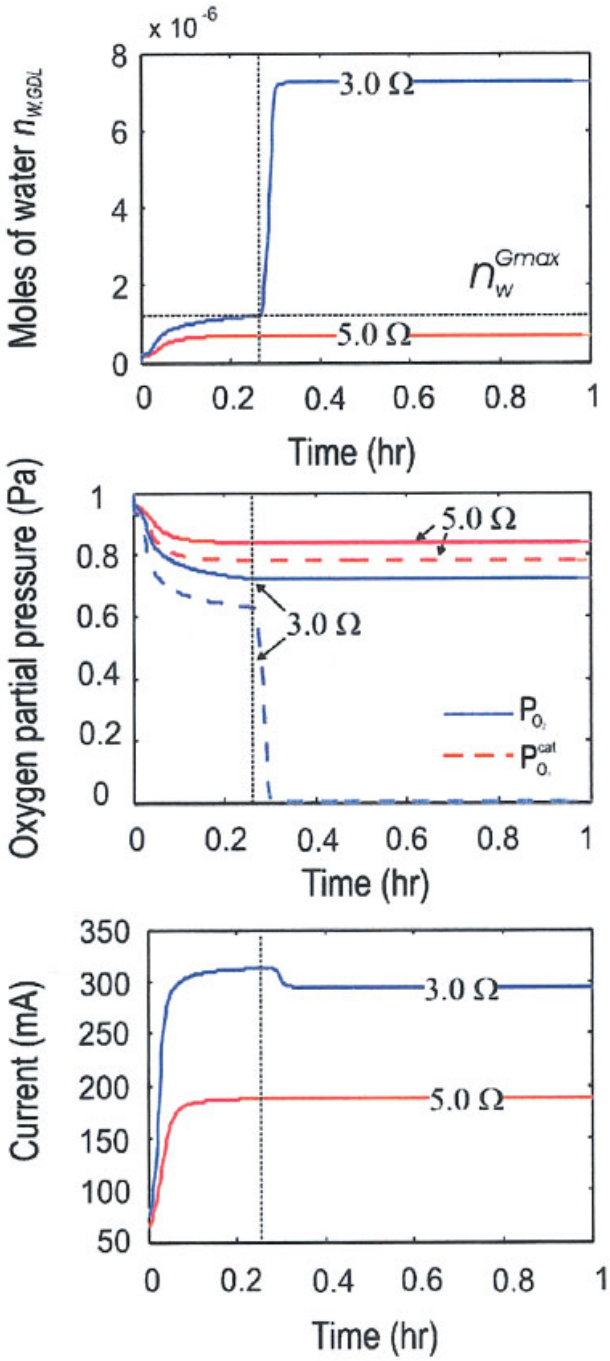

Figure 5. Flooding effects in the cathode.

Transient fuel cell behavior at $R_L = 5\ \Omega$ (dry cathode) and $R_L = 3\ \Omega$ (wet cathode); $T = 353$ K; $F^{in}_A = F^{in}_C = 8.33 \times 10^{-8}$ m^3/s. For the 3 Ω case–(a) Onset of liquid water formation; (b) The presence of liquid water leads to a marked drop in $P^{cat}_{O_2}$, and (c) the current decreases due to limited oxygen supply to the catalyst surface. [Color figure can be viewed in the online issue, which is available at www.interscience.wiley.com.]

Computational Results

The Single STR-PEM Fuel Cell with GDL Flooding. The STR-PEM fuel cell will ultimately approach different steady-states depending on the initial and operating conditions. Increasing the temperature would increase the rate of

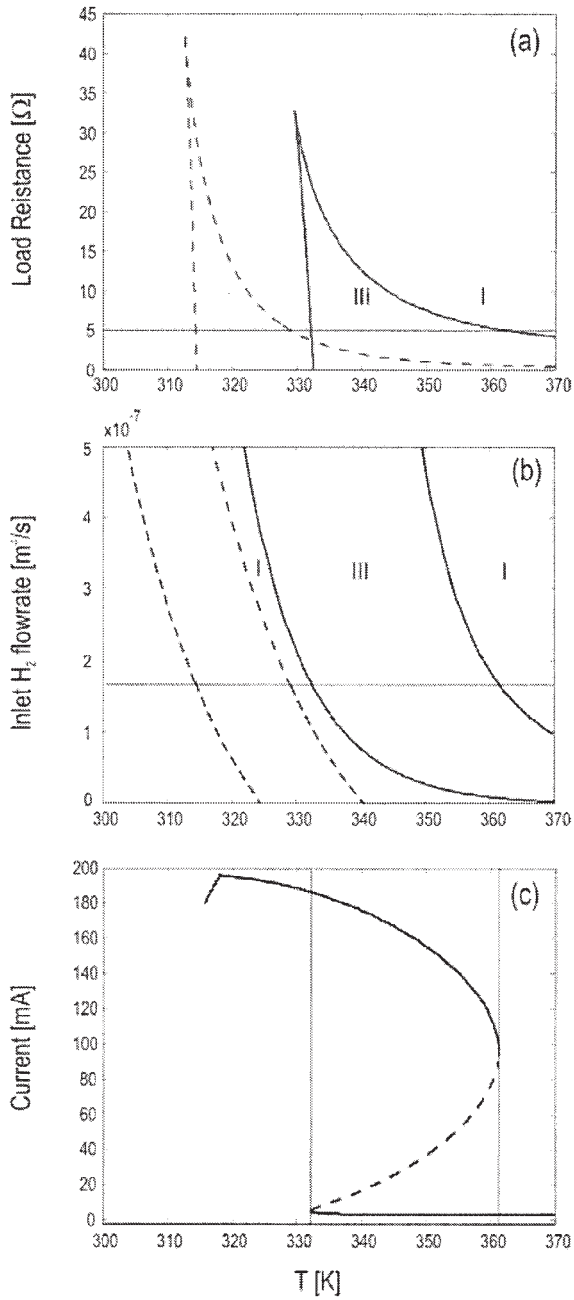

Figure 6. Two-parameter bifurcation diagrams for the single STR-PEM fuel cell with GDL flooding.

(a) T and R_L [$F_A^{in} = 1.67 \times 10^{-7}$ m^3/s, $F_C^{in} = 2.5 \times 10^{-7}$ m^3/s], (b) T and F_A^{in} [$F_C^{in} = 2.5 \times 10^{-7}$ m^3/s, $R_L = 5\ \Omega$], and (c) corresponding one parameter continuation for $R_L = 5\ \Omega$, marked in panel (a) [$F_A^{in} = 1.67 \times 10^{-7}$ m^3/s, $F_C^{in} = 2.5 \times 10^{-7}$ m^3/s]. Solid (dashed) curves denote stable (unstable) steady states. Dashed lines in (a, b): previous model results, not accounting for GDL flooding.

water removal; increasing the load resistance would decrease the rate of water production. In Figure 5, we study a single STR-PEM fuel cell, which has initially been equilibrated to a steady state membrane water content of $a_w = 0.1$. The fuel cell was then set to operate at 353 K with 8.33×10^{-8} m^3/s reactant feed flow rates for two-different load resistances: 5 Ω and 3 Ω. As shown in Figure 5c, a lower steady-state current is achieved when operating the fuel cell at $R_L = 5\ \Omega$ in comparison to $R_L = 3\ \Omega$. Although the 3 Ω case yields a larger steady-state current, partial flooding effects in the cathode GDL impede oxygen transfer to the catalyst surface. The onset of liquid water formation as depicted in Figure 5a is accompanied by a distinct drop in $P_{O_2}^{cat}$ in Figure 5b.

Using the bifurcation/continuation software AUTO,[19] we determined regions of multiplicity in parameter space (the four controllable parameters T, R_L, F_A^{in}, F_C^{in}) for the single STR-PEM fuel cell. The results are presented in three two-parameter bifurcation diagrams (T and R_L in Figure 6a, T and F_A^{in} in Figure 6b, F_C^{in} and F_A^{in} in Figure 7a). Regions of three steady states are marked by III, while regions with a unique steady-state are indicated by I. Bifurcation results from the current model, involving the GDL (solid lines) are plotted in comparison to the results from our previous model described in [39] (dotted line). The multiplicity regions from the current, augmented model correspond more closely to experimentally observed regions in parameter space, suggesting an improvement from our previous modeling work.

Selected one-parameter cuts across the two-parameter diagrams, illustrating the ignition-extinction transitions, are included in Figures 6c and 7b. The solid curves in the one-parameter cuts represent stable steady-states, while the dashed curves represent unstable-steady states. For low-temperatures or low-inlet oxygen flow rates, the current in the upper stable branch is observed to decrease due to the flooding in the cathode GDL. Since the stable-steady states can be determined experimentally, one could generate the stable branches of these one parameter cuts by manually changing one of the controllable parameters slowly. The fuel cell would then be allowed to equilibrate to the new controllable parameter before the current is recorded.

We have also identified regions in parameter space where flooding occurs, via numerical continuation. In Figure 8, the lines represent the "onset of flooding" boundary and correspond to conditions where the water activity in the cathode GDL, a_{gdl} becomes 1. From Figure 8a, we observe that we can avoid flooding by operating the fuel cell with larger inlet oxygen flow rates F_C^{in}. From Figure 8b, we see that the flooded region decreases significantly when the fuel cell temperature is increased. These diagrams indicate that both higher operating temperatures and larger-flow rates facilitate water removal,

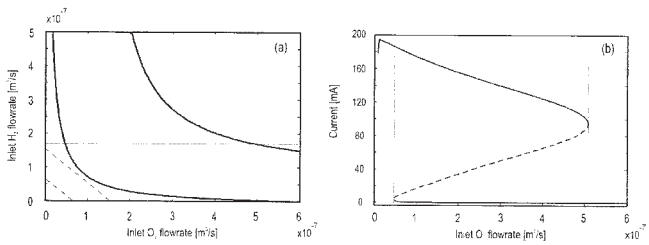

Figure 7. Two parameter bifurcation diagram for the single STR-PEM fuel cell with GDL flooding.

(a) F_A^{in} and F_C^{in} [$T = 353$ K, $R_L = 5\ \Omega$]; the region of steady state multiplicity lies between the curve pairs (curves of saddle-node bifurcations); Dashed lines: previous model results, not accounting for GDL flooding, and (b) representative one parameter continuation in F_C^{in} for $F_A^{in} = 1.67 \times 10^{-7}$ m^3/s as marked in (a).

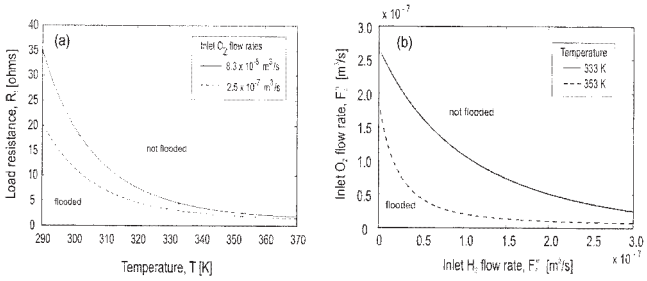

Figure 8. Onset of GDL flooding in parameter space.

(a) T and R_L [$F_A^{in} = 1.67 \times 10^{-7}$ m^3/s], and (b) F_A^{in} and F_C^{in} [$R_L = 5\ \Omega$].

thereby, reducing the flooded region. Overall, the continuation results obtained based on the model are important in helping us determine suitable experimental operating conditions for the fuel cell.

STR-PEM Fuel Cells in Series. In the case of several connected STR-PEM fuel cells, the flow pattern alone can change the current profiles in the tanks. In Figure 9, we present data for two STR-PEM fuel cells connected in series operating under cocurrent flow and countercurrent flow. The fuel cells have been pre-equilibrated to a membrane water content of $a_w = 0.1$ before operating at $T = 353$ K, $R_L = 5\ \Omega$, $F_A^{in} = F_C^{in} = 1.67 \times 10^{-7}$ m^3/s. Under these conditions, although both flow patterns lead to the same total current (155 mA), the current profiles differ significantly. For the cocurrent flow, the current in the second tank evolves to a much larger value (124 mA) in comparison to the current in the first tank (31.2 mA). In contrast, for countercurrent flow, the currents in both tanks evolve closer together and, at steady state, the currents in the first and second tanks are 82 mA and 73.4 mA, respectively. These effects arise because the flow pattern affects the water content in the membrane. The countercurrent flow scheme sustains a higher water content in the fuel cell, since water produced in tank 2 is brought back into tank 1, and successfully prevents the current in tank 1 from extinguishing.

Using several STR-PEM fuel cells in series, we demonstrate that we can alter the ignition locations and form "wet spots" at different locations in the fuel cell array (by analogy to "hot spots" in tubular reactor modeling[40,41]). For a series of six STR-PEM fuel cells in cocurrent flow (at $T = 338$ K, $F_A^{in} = F_C^{in} = 1.33 \times 10^{-7}$ m^3/s), with each tank initially pre-equilibrated at a membrane water content of $a_w = 0.1$, we observe the current evolution for all six tanks under two different loads, $R_L = 6\ \Omega$ and $R_L = 3\ \Omega$. As expected, a larger total current (325 mA) is observed for the smaller load of 3.0 Ω, in contrast to the total current for 6 Ω (157 mA). However, it is interesting to see that the current profiles are very different for the two-load resistance values.

In Figure 10a, the steady-state current is largest in the last tank, and lowest in the first. In contrast, when the tanks are operating at 3 Ω, the steady-state current is smallest in the last tank and largest in tank 2. The difference in the current profiles is the result of different membrane water contents along the cell array. When liquid water is present in the GDL, the water activity at the cathode GDL (a_{gdl}) is 1. At 6 Ω, all six tanks remain dry (no liquid water), but at 3 Ω, partial flooding occurs initially in the last tank, as indicated by the sudden increase in $n_{w,gdl}$ for tank 6 in Figure 10c. The increased liquid water level propagates to tank 5 and subsequently even tanks 4 and 3 flood partially. The steady-state current in tanks 3, 4, 5, and 6 are much lower in comparison to the steady-state current obtainable from these tanks had they remained dry (no liquid water).

The current evolution also differs between the 6 Ω and 3 Ω

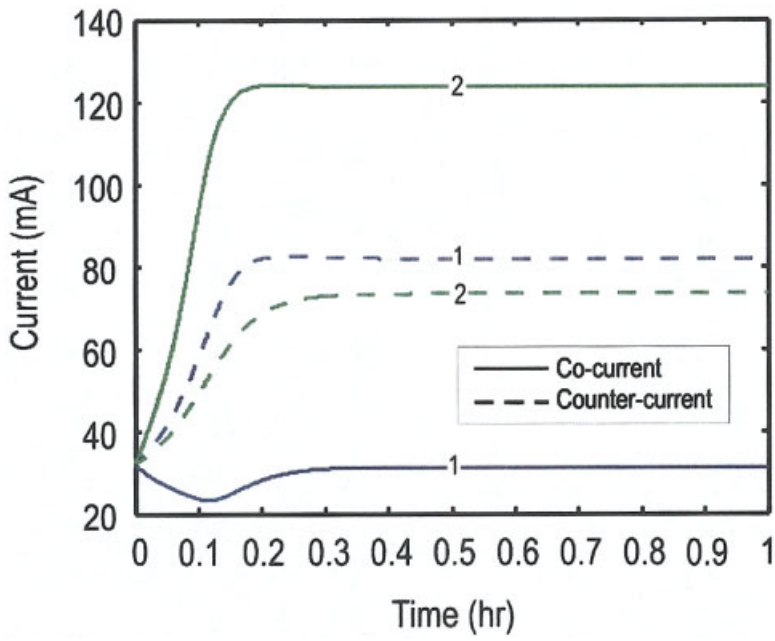

Figure 9. Flow pattern effect on ignition for two STR-PEM fuel cells in series.

[$T = 353$ K; $R_L = 5.0\ \Omega$; $F_A^{in} = 1.67 \times 10^{-7}$ m^3/s; $F_C^{in} = 1.67 \times 10^{-7}$ m^3/s]
Current profiles for tanks 1 and 2 in the cocurrent and countercurrent flow-scheme. [Color figure can be viewed in the online issue, which is available at www.interscience.wiley.com.]

cases in a countercurrent scheme with the same initial membrane water content in each tank ($a_w = 0.1$). For the fuel cell operating at 6 Ω, as shown in Figure 11a, the steady-state currents in all six tanks are smaller in comparison to the currents in Figure 11b. For the lower load resistance of 3 Ω, the steady state currents in the middle of the array (tanks 3, 4 and 5) are lower in comparison to the currents in the tanks at the array ends. In the countercurrent scheme, flooding initially occurs in the middle, beginning in tank 4. Although some tanks are partially flooded, the level of liquid water in them is not enough to completely inhibit oxygen transport to the catalyst (and extinguish the current).

Summary and Discussion

In previous work[39,42] we had shown, through a simplified yet physically reasonable model of the STR-PEM fuel cell, that steady-state multiplicity occurs in the cell due to the autocatalytic nature of the water transport coupled to the water production. Here, we have extended the model so that it retains the multiplicity features of the original model, while accounting for key transport processes in the fuel cell. Incorporating mass-transport processes in the gas-diffusion layer accounts more realistically for current drops resulting from increased mass-transport resistance due to flooding. We have also demonstrated (through both the single and multiple STR-PEM fuel cells in series), that the cathode GDL flooding is marked by an increased level of liquid water, which obstructs the mass transfer of oxygen to the cathode catalyst surface. Multiple tanks in series studies can be used to explore flow pattern effects on the cell dynamics. Using arrays of several tanks in series, we were able to detect current heterogeneities along the cell array; regions of higher-current correspond to wet spots in the fuel cell array. Ignition/extinction phenomena as observed through the updated STR-PEM fuel cell model depend on the controllable parameters (T, R_L, F_A^{in}, F_C^{in}). Parametric continuation computations offer insight into suitable operating parameter settings by identifying the flooding regions in parameter space.

The water balance in the STR-PEM fuel cell is analogous to the heat balance in the autocatalytic CSTR. By extending our *differential* model to the tanks in series scheme, we are able to mimic the *integral* reactor; we see that the flow pattern alone is capable of determining whether or not the fuel cell can sustain a sufficient level of water to ensure ignition (operation at a high steady-state current). We have demonstrated the occurrence of high water content regions within the STR-PEM fuel cell (wet spots) that are directly analogous to high-temperature regions (hot spots) in the classic tubular reactor. Changing the flow pattern—in addition to manipulating the controllable parameters—can alter the spatial location of the transient ignitions, as well as the ultimate steady-state current pattern in a cell array. Initial experimental observations appear to support these theoretical predictions.[13,34]

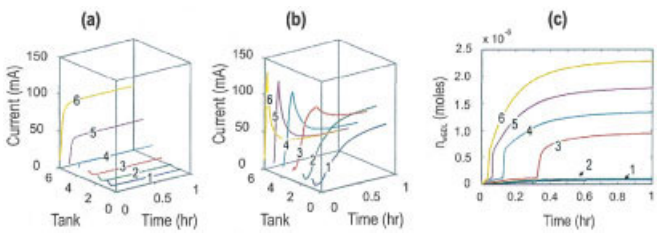

Figure 10. Six tanks in *cocurrent* flow.

Transient current profiles (T = 338 K; $F_A^{in} = F_C^{in} = 1.33 \times 10^{-7}$ m^3/s) in each tank for: (a) $R_L = 6$ Ω, all tanks remain dry; (b) $R_L = 3.0$ Ω, current decreases in the end tanks, and (c) $R_L = 3$ Ω, liquid water formation occurs initially in the tanks at the outflow end. [Color figure can be viewed in the online issue, which is available at www.interscience.wiley.com.]

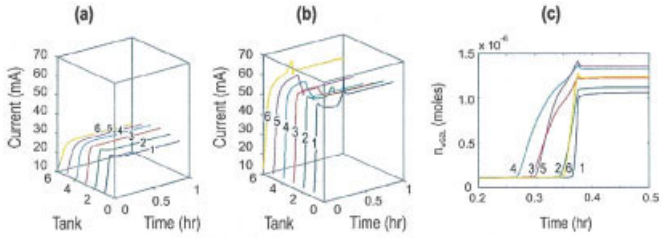

Figure 11. Six tanks in *countercurrent* flow.

Transient current profiles (T = 338 K; $F_A^{in} = F_C^{in} = 1.33 \times 10^{-7}$ m^3/s) in each tank for (a) $R_L = 6$ Ω: all tanks remain dry, (b) $R_L = 3$ Ω current decreases in the middle tanks, and (c) $R_L = 3$ Ω: liquid water first forms in the tanks in the middle. [Color figure can be viewed in the online issue, which is available at www.interscience.wiley.com.]

Acknowledgments

The authors acknowledge support through the AFOSR (Dynamics and Control), National Science Foundation (CTS-0354279 and DMR-0213707). E. Chia thanks the Princeton University Program in Plasma Science and Technology and the U.S. Department of Energy Contract No. DE-AC02-76-CHO-3073 for fellowship support.

Notation

A = electrode/electrolyte interfacial area, 1.5×10^{-4} m^2
$A_{(j)}$ = j^{th} segment electrode/electrolyte interfacial area, (A/N) m^2
A_m = cross-sectional area of electrolyte membrane for longitudinal water transport, 1×10^{-6} m^2
a_w = activity of water in membrane
a_w^{GDL} = activity of water in cathode gas diffusion layer
$\mathcal{F}$ = Faraday's constant, 96,500 coulombs/mol
F_A = Flow rate at the anode, m^3/s
F_C = Flow rate at the cathode, m^3/s
i = current, A
I_o = saturation current, 2×10^{-3} A
k = mass-transfer coefficient from membrane to anode flow channel, 1.3×10^{-2} mol/m^2-s
k' = mass-transfer coefficient from cathode GDL to membrane, at 5.6×10^{-2} mol/m^2-s
k'' = mass-transfer coefficient from the GDL to the cathode flow channel, 1.6×10^{-2} mol/m^2-s
k_A = hydrogen mass-transfer coefficient at anode, 5.8×10^{-6} mol/m^2-s-Pa
k_C = oxygen mass-transfer coefficient at cathode, mol/m^2-s-Pa
$k_c^{\max}$ = maximum oxygen mass-transfer coefficient at cathode GDL, 5.8×10^{-7} mol/m^2-s-Pa
$k_c^{\min}$ = minimum oxygen mass-transfer coefficient at cathode GDL, 5.8×10^{-10} mol/m^2-s-Pa
k_m = mass-transfer coefficient for water transport through the membrane, 0.5 mol/m^2-s
k_w^{eo} = $2(P_{wA}/P_{wo})^4$, electro-osmotic drag coefficient
λ = number of water molecules absorbed per sulfonic acid group
n_w^L = moles of liquid water in the cathode gas diffusion layer
$n_w^{\max}$ = molar capacity of water in the GDL, 8.3×10^{-4} mol
N_{SO3} = number of sulfonic acid groups in membrane, 3.5×10^{-5} mol
P_{H2} = hydrogen pressure in gas flow channel, Pa
P_{O2} = oxygen pressure in gas flow channel, Pa
P_{wA} = water partial pressure in anode flow channel, Pa

P_{wC} = water partial pressure in the cathode flow channel, Pa
P_{wo} = vapor pressure of water a fuel cell temperature, Pa
P_T = total pressure, 10^5 Pa
R = gas constant
R_L = external load resistance, Ω
R_M = internal resistance of membrane electrode assembly, Ω
T = fuel cell temperature, K
V_g^A, V_g^C = flow channel volume associated with differential element, 2×10^{-7} m^3
V_{FC} = local potential difference between anode and cathode, V
V_o = standard state fuel cell voltage, 1.23 V
V_T = electrode/electrolyte interface threshold voltage, 0.05 V

Literature Cited

1. EG&G Services P, Inc. *Fuel Cell Handbook* 5th ed. Morgantown: U.S. Department of Energy; 2000.
2. Acres GK. Recent advances in fuel cell technology and its applications. *J Power Sources.* 2001;100:60–66.
3. Perry ML, Fuller TF. A Historical Perspective of Fuel Cell Technology in the 20th Century. *J Electrochem Soc.* 2002;149(7):S59–S67.
4. Bernardi DM, Verbrugge MW. A Mathematical-Model of the Solid-Polymer-Electrolyte Fuel-Cell. *J of the Electrochem Soc.* 1992;139(9): 2477–2491.
5. Janssen GJ. A phenomenological model of water transport in a proton exchange membrane fuel cell. *J Electrochem Soc.* 2001;148:A1313.
6. Springer TE, Zawodzinski TA, Gottesfeld G. Polymer electrolyte fuel-cell model. *J Electrochem Soc.* 1991;138:2334.
7. Fuller TF, Newman J. Water and Thermal Management in Solid-Polymer-Electrolyte Fuel-Cells. *J Electrochem Soc.* 1993;140:1218.
8. Pisani L, Murgia G, Valentini M, D'Aguanno B. A working model of polymer electrolyte fuel cells. *J Electrochem Soc.* 2002;149(7):A898–A904.
9. Moxley JF, Tulyani S, Benziger JB. Steady-state multiplicity in the autohumidification polymer electrolyte membrane fuel cell. *Chem Eng Sci.* 2003;58(20):4705–4708.
10. Benziger J, Chia E, Karnas E, Moxley J, Teuscher C, Kevrekidis IG. The stirred tank reactor polymer electrolyte membrane fuel cell. *AIChE J.* 2004;50(8):1889–1900.
11. Chia ESJ, Benziger JB, Kevrekidis IG. Water balance and multiplicity in a polymer electrolyte membrane fuel cell. *AIChE J.* 2004;50(9): 2320–2324.
12. Benziger J, Chia E, Moxley JF, Kevrekidis IG. The dynamic response of PEM fuel cells to changes in load. *Chem Eng Sci.* 2005;60(6):1743–1759.
13. Benziger JB, Chia JE, Kevrekidis IG. Ignition and front propagation in polymer electrolyte membrane fuel cells. *J Phys Chem B.* 2006; submitted.
14. Aris R. *Introduction to the Analysis of Chemical Reactors.* Englewood Cliffs: Prentice-Hall; 1965.
15. van Heerden C. Autothermic processes: Properties and reactor design. *Ind Eng Chem.* 1953;45:1242.
16. Perlmutter DD. *Stability of Chemical Reactors.* Englewood Cliffs: Prentice-Hall; 1972.
17. Uppal A, Ray WH, Poore AB. Dynamic behavior of continuous stirred tank reactors. *Chem Eng Sci.* 1974;29:967.
18. Schmitz RA. Multiplicity, stability, and sensitivity of states in chemically reacting systems—A Review. *Chem Eng Rev.* 1975;148:156.
19. Doedel EJ. AUTO: A Program for the Automatic Bifurcation Analysis of Autonomous Systems. Paper presented at: *Proceedings 10th Manitoba Conference on Numerical Mathematics and Computation,* Winnipeg; 1981.
20. Farr WW, Aris R. Yet who would have thought the old man to have had so much blood in him: Reflections on the multiplicity of steady-states of the stirred tank reactor. *Chem Eng Sci.* 1986;41:1385.
21. Balakotaiah V, Luss D. Exact steady-state multiplicity criteria for 2 consecutive or parallel reactions in lumped-parameter systems. *Chem Eng Sci.* 1982;37(3):433–445.
22. Balakotaiah V, Luss D. Structure of the steady-state solutions of lumped-parameter chemically reacting systems. *Chem Eng Sci.* 1982b; 37:1611.
23. Jeng KT, Lee SF, Tsai GF, Wang CH. Oxygen mass transfer in PEM fuel cell gas diffusion layers. *J Power Sources.* 2004;138:41–50.
24. Lin G, He W, Nguyen TV. Modeling liquid water effects in the gas diffusion and catalyst layers of the cathode of a PEM fuel cell. *J Electrochem Soc.* 2004;151(12):A1999–A2006.
25. Pasaogullari U, Wang CY. Liquid water transport in gas diffusion layer of polymer electrolyte fuel cells. *J Electrochem Soc.* 2004; 151(3):A399–A406.
26. Eikerling M, Kornyshev AA, Stimming U. Electrophysical properties of polymer electrolyte membranes: A random network model. *J Phys Chem B.* 1997;101:10807.
27. Hsu WY, Gierke TD. Ion clustering and transport in nafion perfluorinated membranes. *J Electrochem Soc.* 1982;129:C121.
28. Thampan T, Malhotra S, Tang H, Datta R. Modeling of conductive transport in proton-exchange membranes for fuel cells. *J Electrochem Soc.* 2000;147:3242.
29. Paddison SJ. The modeling of molecular structure and ion transport in sulfonic acid based ionomer membranes. *J New Mat Electrochem Systems.* 2001;4:197.
30. Yang CR. *Performance of Nafion/Zirconium Phosphate Composite Membranes in PEM Fuel Cells.* Princeton: Department of Mechanical Engineering, Princeton University; 2003.
31. Yang CR, Srinivasan S, Bocarsly AB, Tulyani S, Benziger JB. A comparison of physical properties and fuel cell performance of nafion and zirconium phosphate/nafion composite membranes. *J Memb Sci.* 2004;237:145–161.
32. Springer TE, Zawodzinski TA, Gottesfeld S. Polymer electrolyte fuel-cell model. *J of the Electrochem Soc.* 1991;138(8):2334–2342.
33. Webb D, Moller-Holst S. Measuring individual cell voltages in fuel cell stacks. *J of Power Sources.* 2001;103(1):54–60.
34. Benziger J, Chia E, Kimball E, Kevrekidis I. Reactor dynamics of parallel flow channel PEM fuel cells. *AIChE J.* 2006;submitted.
35. Zawodzinski TA, Derouin C, Radzinski S, Sherman RJ, Smith VT, Springer TE, Gottesfeld S. Water-uptake by and transport through nafion(R) 117 membranes. *J of the Electrochem Soc.* 1993;140(4): 1041–1047.
36. Eikerling M, Kharkats YI, Kornyshev AA, Volfkovich YM. Phenomenological theory of electro-osmotic effect and water management in polymer electrolyte proton-conducting membranes. *J of the Electrochem Soc.* 1998;145(8):2684–2699.
37. Choi KH, Peck DH, Kim CS, Shin DR, Lee TH. Water transport in polymer membranes for PEMFC. *J of Power Sources.* 2000;86(1–2): 197–201.
38. Hogarth WHJ, Benziger JB. Dynamics of Autohumidified PEM Fuel Cell Operation. *J of the Electrochem Soc.* 2006;153(11); DOI 10.1149/1.2344841.
39. Chia EJ, Benziger JB, Kevrekidis IG. Water balance and multiplicity in a polymer electrolyte membrane fuel cell. *AIChE J.* 2004;50(9): 2320–2324.
40. Froment GF. Fixed bed catalytic reactors—current design status. *Ind Eng Chem.* 1967;59(2):18.
41. Luss D. Temperature fronts and patterns in catalytic systems. *Ind & Eng Chem Res.* 1997;36(8):2931–2944.
42. Benziger JB, Chia EJ, Karnas E, Moxley J, Teuscher C, Kevrekidis IG. The stirred tank reactor polymer electrolyte membrane fuel cell. *AIChE J.* 2004;50(8):1889–1900.

Manuscript received Dec. 6, 2005, and revision received July 26, 2006.